The expected neutrino signal from the formation of black holes via protoneutron star collapse

Tobias Fischer[1] [2], **Matthias Liebendörfer**[2] **and Anthony Mezzacappa**[3]

Abstract. We discuss the formation of stellar mass black holes via protoneutron star (PNS) collapse. Such PNSs are modelled as central objects in general relativistic 1D core collapse simulations with Boltzmann neutrino transport. In the absence of an earlier explosion, the PNS collapses eventually due to continued accretion of outer layers of a massive star onto the central object. We investigate the resulting conditions with respect to neutrino emission at the formation of a black hole.

1. Introduction

Black hole formation via neutron star collapse has been investigated by many authors, even in multi-dimensional general relativistic context. On the other hand, the uncertainties about the input physics for neutron stars at high densities and temperatures are large and because the coupling to neutrino transport is complicated, most hydrodynamical models have been performed adiabatically based on a polytropic equation of state (EoS). The present article follows an alternative approach and reports on black hole formation via spherically symmetric protoneutron star (PNS) collapse, including sophisticated input physics [Lattimer and Swesty (1991), Bruenn (1985)] as well as neutrino transport, similar to work by Baumgarte et al. (1996) and Sumiyoshi et al. (2006).

If the nuclear burning process of massive stars reaches iron group nuclei, photodisintigration and electron capture on protons and nuclei reduce the mostly electron supported pressure and the central core of the star starts to contract. The inner part of the stellar core collapses subsonically while the outer part collapses super-sonically. The collapse continues until nuclear densities $\sim 2 \times 10^{14} g/cm^3$ are reached and the core bounces back (depending on the EoS). Neutrinos produced during collapse, mostly ν_e via electron captures on free protons and nuclei, are able to leave the star until neutrino trapping densities are reached. The large number of electron captures is reflected in the ν_e luminosity increase before bounce, while the production of all other neutrino flavors $(\bar{\nu}_e, \nu_{(\mu,\tau)}, \bar{\nu}_{(\mu,\tau)})$ is suppressed in the cold, electron-degenerate matter. Right after bounce, a sound wave steepens to a shock front and propagates outwards with positive velocities, lasting from the energy transfer at bounce. Outer layers of the star continue to fall onto that shock front. However, due to dissociation and neutrino losses, the shock quickly turns into an accretion front which expands to about $150\,km$ after a few $100\,ms$ (depending on the progenitor star and the EoS). The idea of reviving this stalled shock again via neutrino

[1] Project funded by the Swiss National Foundation, grant no. 106627
[2] Department of Astronomy and Physics, University of Basel, Klingelbergstrasse 82, 4057 Basel
[3] Physics Division, Oak Ridge National Laboratory, Oak Ridge, Tennessee 37831-1200

reactions behind the shock, such as absorption and scattering, has long been investigated as the possible explosion mechanism of a massive star [Bethe and Wilson (1985), see e.g. Mezzacappa et al. (2004)]. In the dissociated matter behind the shock, ν_e and $\bar{\nu}_e$ captures are the dominant heating reactions. In the accreting matter ahead of the shock, Bruenn and Haxton (1991) found the dominant neutrino-fluid interactions are ν_e-nucleus absorption and neutrino-electron scattering, which may preheat the unshocked material. However, the absence of any explosion in 1D core collapse models of stars more massive then $11\,M_\odot$, advises the conjecture that important physical ingredients are missing, most likely multi-dimensional phenomena such as convection and rotation [Herant et al. (1994), Burrows et al. (1995), Buras et al. (2006), Bruenn et al. (2006)].

On the other hand, the lack of an explosion makes it possible to explore accretion phenomena. If the mass of the accreting PNS exceeds the critical limit, neutron pressure and nuclear forces are not able to keep the PNS stable and the PNS starts to collapse until the event horizon is formed. The accretion time until PNS collapse lasts from several $100\,ms$ up to several s, depending on the stiffness of the EoS at supranuclear densities and the accretion rate set up by the progenitor model. The PNS collapse to a black hole itself happens on a much shorter time scale of a few ms.

The paper is organised as follows. Section 2 is devoted to an overview of our general relativistic hydrodynamics and neutrino transport model [Lindquist (1966), Mezzacappa and Bruenn (1993a-c), Liebendörfer et al. (2001ab, 2004)]. In section 3, we will discuss the final state of a core collapse supernova simulation of a $40\,M_\odot$ progenitor from Woosley et al. (2002), where the lack of an explosion and the continued accretion of matter onto the PNS as central object eventually leads to the collapse of the PNS to a black hole. Special attention is thereby devoted to the neutrino signal in section 4 (see for example ref. Wilson (1971), Burrows (1988)).

2. 1D general relativistic hydrodynamics and neutrino transport

Our model is based on an implicit three-flavor neutrino and anti-neutrino Boltzmann transport solver developed by Mezzacappa and Bruenn (1993a-c), describing the neutrino transport as well as microphysical interactions between neutrinos and the fluid [Schinder and Shapiro (1982), Bruenn (1985), Mezzacappa and Messer (1999)]. In order to treat the postbounce phase, this Lagrangian model was coupled to an implicit general relativistic hydrodynamics code that features an adaptive grid [Liebendörfer et al. (2001b)]. Additionally, the neutrino Boltzmann solver has been extended to solve the general relativistic transport equations described by Lindquist (1966). Special emphasis has been given to implement a finite differencing of the coupled transport and hydrodynamics equations that accurately conserves lepton number and energy in the postbounce phase [Liebendörfer et al. (2001a, 2004)]. This approach has been analytically generalised to the formulation of a conservative general relativistic kinetic theory in multiple spatial dimensions by Cardall and Mezzacappa (2003).

The core collapse of a massive star is a non-stationary and (in the most simple approximation) spherically symmetric process. In this case, the spacetime can be described with the following line element

$$ds^2 = \alpha(t,a)^2 dt^2 + \frac{r'(t,a)^2}{\Gamma(t,a)^2} da^2 + r(t,a)^2 (d\theta^2 + \sin^2\theta d\phi^2)$$

with coordinates as follows: t time, a baryon number or mass. $r(t,a)$ is the radius of the 2-sphere with angles (θ,ϕ). The prime denotes spatial derivatives with respect to a. Interior solutions of the Einstein equation are obtained in terms of differential equations in t and a for the metric functions $\alpha(t,a)$ (lapse function) and $\Gamma(t,a)$ (see for example the early analytical work by Misner and Sharp (1964) and relativistic core collapse simulations by May and White (1967)). In analogy to approaches in Newtonian hydrodynamics, the conservation equation for energy ${T_t}^{\mu}{}_{;\mu} = 0$ and momentum ${T_a}^{\mu}{}_{;\mu} = 0$ are solved to determine the dynamics of the collapsing star.

The stress-energy tensor of a collapsing star taking care of the fluid dynamics, neutrino transport and microphysical interactions between the fluid and neutrinos can be written as follows

$$T_t{}^t = \rho(1 + e + J)$$
$$T_a{}^t = \rho H$$
$$T_a{}^a = p + \rho K$$
$$T_\theta{}^\theta = T_\phi{}^\phi = p + \frac{1}{2}\rho(J - K),$$

with isotropic fluid pressure p, rest mass energy density ρ, internal specific fluid energy e, specific radiation energy J and energy flux ρH, which is the first angular momentum of the specific radiation intensity. J and K denote the zeroth and second angular moments of the specific radiation intensity respectively (for a detailed overview, see Lindquist (1966)). This from of the stress-energy tensor reflects, that the energy contents of spacetime is determined by fluid properties as well as by neutrino properties, both contributing to the differential equations for the metric functions. More generally expressed, it is possible to write the stress-energy tensor as a sum of two terms,

$$T_\mu{}^\nu = F_\mu{}^\nu + N_\mu{}^\nu,$$

with

$$N^{\nu\mu} = \int d^3p\, p^\nu p^\mu f(t, \vec{x}, \vec{p}),$$

such that $F_\mu{}^\nu$ determines the fluid energy contents and $N_\mu{}^\nu$ the neutrino energy contents of spacetime. $p^\mu = (\epsilon, \vec{p})$ is the neutrino 4-momentum and ϵ is the neutrino energy. Lindquist (1966) demonstrated the equivalence between the covariant derivative of the neutrino stress-energy tensor to the 3-momentum integrated left hand side of the Boltzmann equation. Therefore, to fulfil $T^{\mu\nu}_{\ ;\nu} = 0$, the following expression holds

$$N^{\mu\nu}_{\ ;\nu} = \int d^3p\; p^\mu\, \Omega = -F^{\mu\nu}_{\ ;\nu},$$

with collisional term Ω, describing microphysical interactions between the fluid and the neutrinos. In the most simple approximation, $\Omega = 0$ if the neutrino distribution function f at any time equals the equilibrium distribution function. Otherwise, the collisional integral for neutrino-matter interactions during a stellare core collapse was found by Yueh and Buchler (1975) to be e.g.

$$\Omega = (1 - f)\, j - \chi\, f + (1 - f) \int d\epsilon' dk'\, f' \int_0^{2\pi} d\phi R^{in}(\epsilon, \epsilon', k, k', \phi)$$
$$-f \int d\epsilon' dk' (1 - f') \int_0^{2\pi} d\phi\, R^{out}(\epsilon, \epsilon', k, k', \phi).$$

Here, ϵ is the neutrino energy and k the propagation direction. The first two terms of Ω determine the change in the neutrino distribution function due to emission and absorption by the emissivity j and the opacity χ. The second two terms give an example for a scattering integral based on the scattering kernels $R^{in/out}$ as given in Mezzacappa and Bruenn (1993c) Appendix A, based on work by Yueh and Buchler (1975, 1977). The primed integral is performed over the distribution function f' of incoming neutrinos in the third term and over outgoing neutrinos in the fourth term.

The equation of state (EoS) used in the simulations is the EoS from Lattimer and Swesty (1991). A detailed description of the model including as well various aspects of black hole formation can be found in Liebendörfer et al. (2004). An investigation similar to the present article, but comparing two different EoS, from Lattimer and Swesty (1991) and from Shen et al. (2001), has been presented recently by Sumiyoshi et al. (2006).

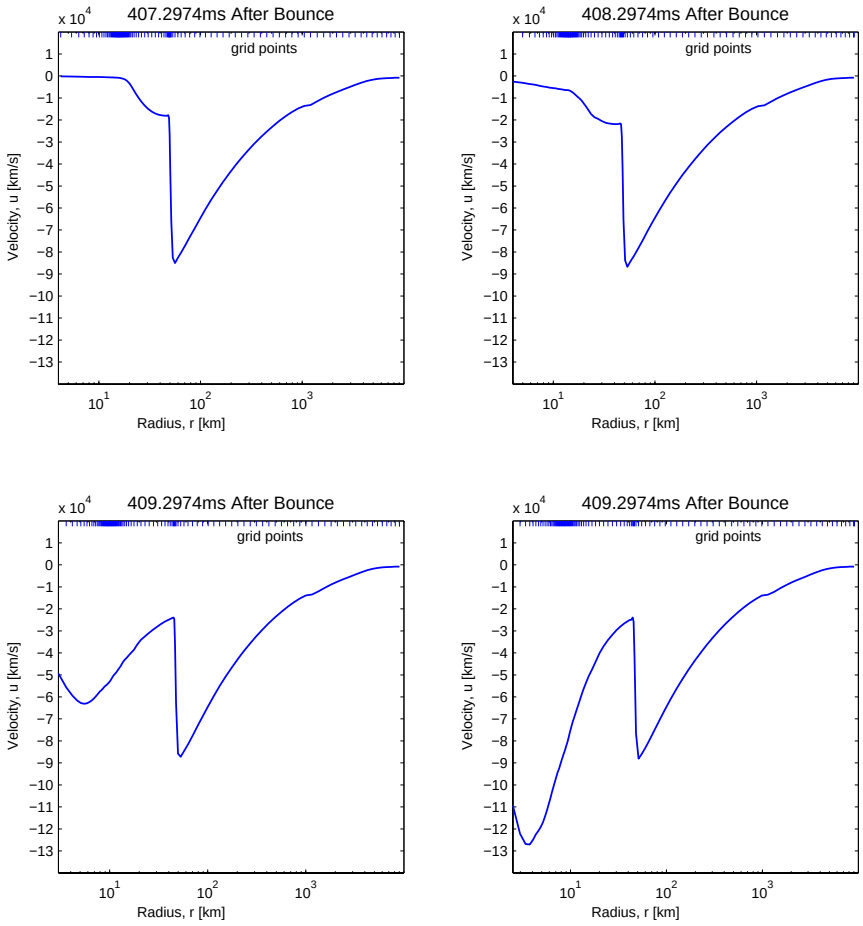

Figure 1.
The graphs show different velocity profiles from the post-bounce phase of a $40\,M_{\odot}$ progenitor from Woosley et al. (2002) during PNS collapse, from stationary accretion (top left panel) to starting collapse (top right and lower left panel) until black hole formation (lower right panel). The accretion front at $50\,km$ radius barely moves on the PNS collapse timescale but loses the pressure support from below.

3. Black hole formation

After the shock front has developed to an accretion front, outer layers of the inner core are decelerated at the shock and continue to drift inwards where they accumulate on the central PNS. Thereby, heavy nuclei dissociate into light nuclei, protons and neutrons, reducing the thermal energy gained from the conversion of kinetic infall energy at the accretion front. The accretion rate onto the PNS is rapidly decreasing with time and the PNS compactifies slowly at timescales from several $100\,ms$ up to several s (depending on the progenitor and the EoS).

Bethe and Wilson (1985) and Janka et al. (2005) have demonstrated, that during the accretion phase, heating via neutrino absorption and scattering processes behind the shock seem most important to revive the stalled shock again. On the other hand, it has not been shown, that the energy deposition from neutrinos into the fluid via absorption and scattering in 1D-models, even including advanced input physics and Boltzmann neutrino transport, is efficient enough to revive the shock and explode non-rotating stars more massive then $11\,M_{\odot}$. Alternative scenarios are investigated, see for example Akiyama et al. (2003) or Burrow et al. (2006). In spherical models, where explosions are absent, the continuous accretion of matter

leads to inwards propagation of the shock front and the PNS grows in mass and compactifies. If the central mass exceeds the critical limit of $\sim 2.0\,M_{\odot}$, gravity exceeds the neutron pressure and nuclear forces, and the PNS starts to contract. The velocity profiles of a PNS collapse launched from a $40\,M_{\odot}$ progenitor star from Woosley et al. (2002) are displayed in figure 1. The collapse happens in a similar manner as the pre-bounce collapse of the progenitor. Differences do occur with respect to the physical scales: The highest infall velocities reach of order c, where c is the speed of light, as well as temperatures above $190\,MeV$. In addition, the density of the central regions exceed $5 \times 10^{15} g/cm^3$. The last configuration of the PNS collapse before black hole formation is shown in figure 2. The physical conditions assumed during PNS collapse are unique as illustrated in figure 2 and though the dynamical evolution is clear, there are significant uncertainties concerning the input physics of PNSs at these extreme conditions such as, for example, the EoS and the neutrino physics (for details, see Beacon et al.(2001) and Thompson and Burrows (2006)). The collapse continues until finally the event horizon is formed at timescales less than a few ms after the PNS has started to contract (see figure 1 as well). In other words, the lapse function $\alpha(t, a) = 0$ at a radius less than $2\,km$ such that a signal emitted at the horizon would need infinite time to leave the star. In our case, the PNS collapse until black hole formation lasts $2\,ms$ only.

In addition, figure 3 shows accretion profiles for velocity, density, entropy and luminosity for two initially different progenitors during the accretion phase. The different profiles from the two models show striking similarities. However, in the initial accretion phase, the shock front of the $15\,M_{\odot}$ progenitor starts to recede slightly earlier than the $40\,M_{\odot}$ progenitor shock front does (figure 3). This can be understood in the less energetic shock front of the less massive model. On the other hand, the less massive one is determined by a lower accretion rate onto the central PNS. In other words, the $40\,M_{\odot}$ model takes over the $15\,M_{\odot}$ model with respect to compactification during the accretion phase. Thus, PNSs as central objects in core collapse simulations of more massive progenitors reach their critical mass much faster than less massive ones. When PNSs reach their critical mass, the resulting objects do hardly differ and the PNS collapse to a black hole is likely to happen in the same way for initially different progenitors.

4. The neutrino signal

The electron neutrino signal during the core collapse simulation launched from a $40\,M_{\odot}$ progenitor of Woosley et al. (2002) is illustrated in figure 4. The peak in the luminosity a few ms after bounce, the so called neutrino burst, represents the release of the neutrinos produced by sustained e^--capture, when the density of the shock-heated material behind the accretion front drops below neutrino trapping density. Later in the post-bounce phase, the region between the neutrino-spheres and the shock has become highly deleptonized. This is reflected in the low Y_e (electron fraction) and the $(\nu_e, \bar{\nu}_e)$-luminosity increase, since their production rates increase. On the other hand, the physical conditions during the final accretion phase favour the generation of (μ, τ)-neutrinos as well as their anti-neutrinos. The traditional pair-production process is

$$e^- + e^+ \leftrightarrows \nu_{(e,\mu,\tau)} + \overline{\nu}_{(e,\mu,\tau)}.$$

Additional (μ, τ)-neutrino as well as their anti-neutrino emission and thermalisation processes have been investigated by Thompson et al. (2001), such as nucleon-nucleon-bremsstrahlung, which has been included into our code by Messer and Bruenn (2003). Buras et al. (2003) pointed out the importance of further (μ, τ)-neutrino pair production via the annihilation of trapped electron flavor neutrino pairs, which is not included yet.

Here we extended the investigations of Liebendoerfer et al. (2004), §2.3 into the significant increase of the (μ, τ)-neutrino and anti-neutrino luminosities after $250\,ms$ post-bounce shown in figure 4. The evolution of the neutrino luminosities in figure 4 depends on the production rates

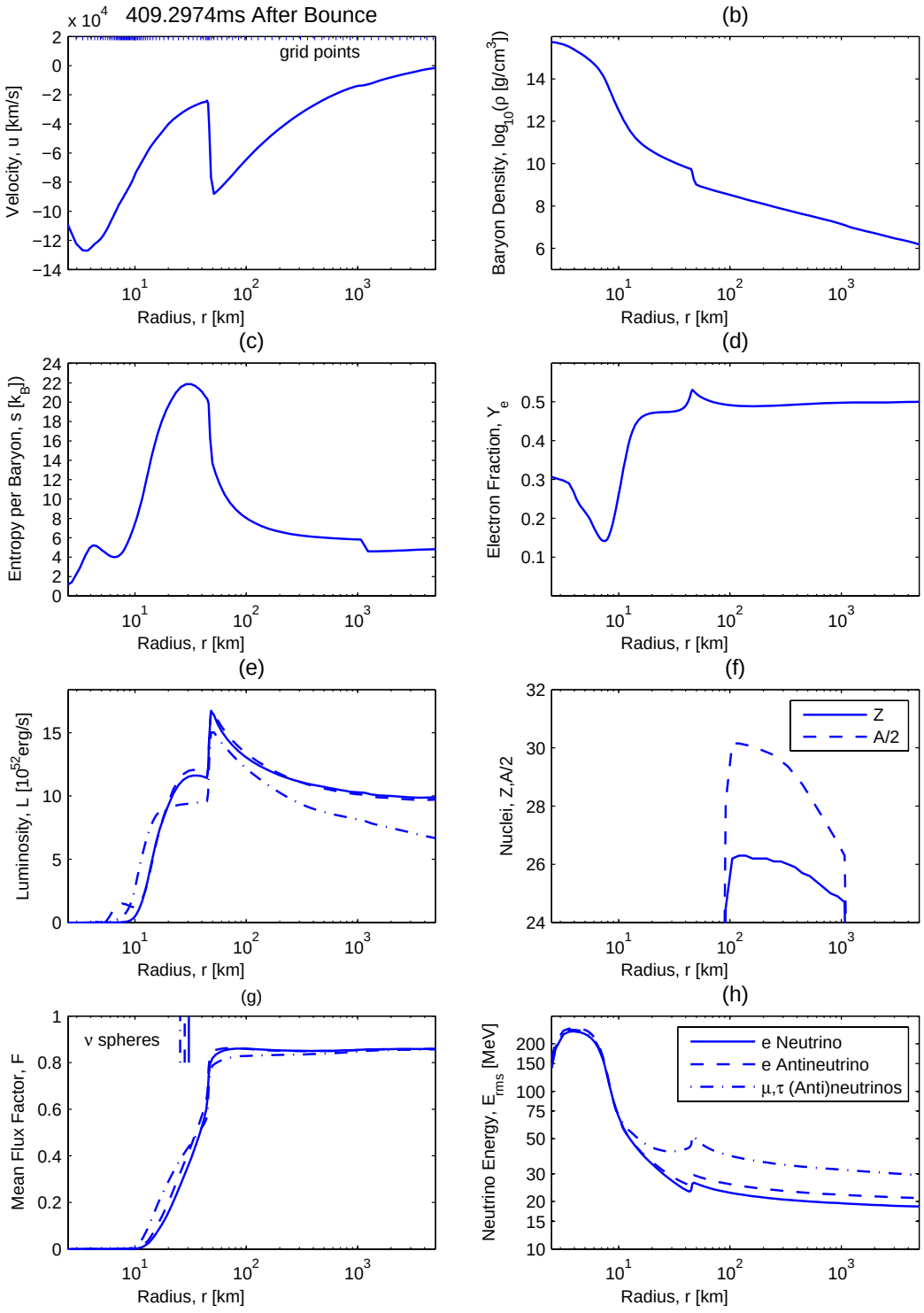

Figure 2.
The graphs show the last configuration during PNS collapse at 409 *ms* after bounce, i.e. at black hole formation.

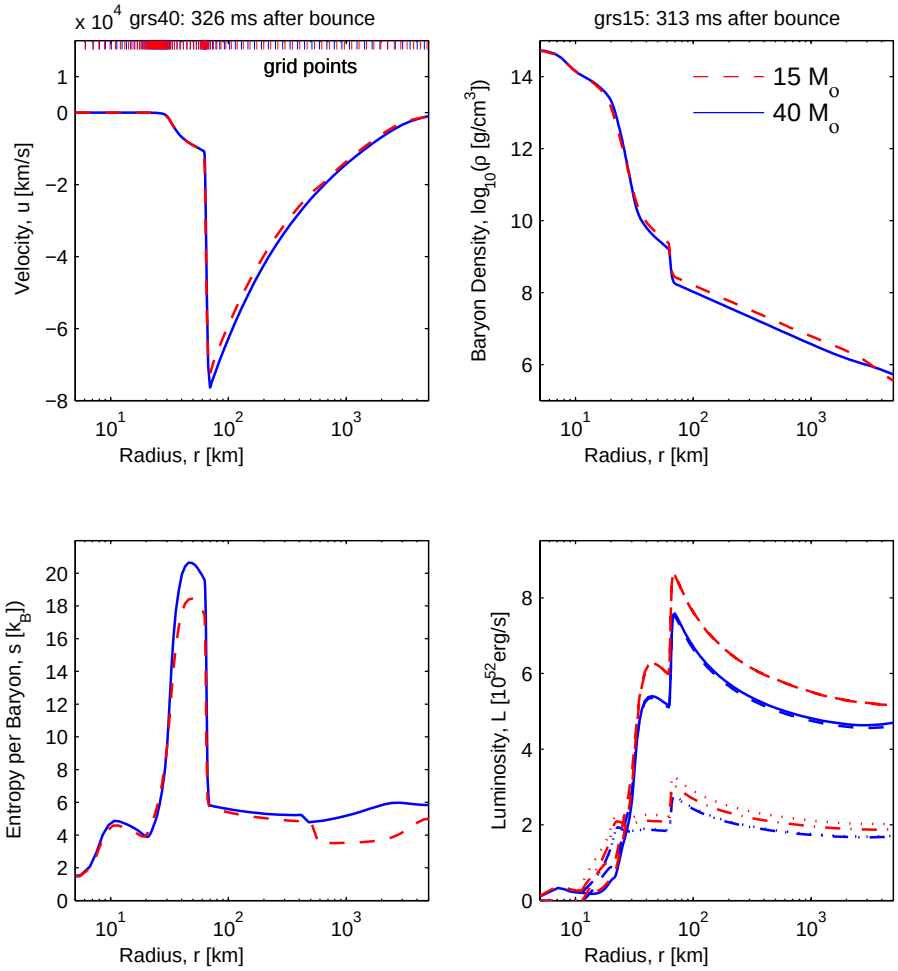

Figure 3.
The graphs show two different models at slightly different times during the initial accretion phase, a $15\,M_\odot$ model at $313\,ms$ after bounce and a $40\,M_\odot$ model at $326\,ms$ after bounce. The profiles are almost identical, especially with respect to the accreting matter onto the central PNS and the PNS interior, but slight differences occur in the accretion rates and time scales.

and the diffusion timescale, which depend on the assumed matter conditions. These conditions and production rates for all neutrino flavors are investigated in figure 5 . The electron flavor neutrinos are produced at lower densities than the (μ, τ)-neutrino pairs, because the latter do not interact via charged current reactions. In order to separate these different regimes, we plot in figure 5 all quantities with respect to the logarithmic baryon density.

The (μ, τ)-pair-neutrino luminosity can be understood as follows: after the shock has stalled, the continued accretion leads to a compactification of the central layers of the stellar core. The temperature increases slowly but constantly, which is reflected in the thermal spectrum of the photons. These thermal photons are in equilibrium with the fluid via

$$e^- + e^+ \leftrightarrows 2\gamma,$$

and therefore the number of (e^-, e^+)-pairs and trapped (ν_e, $\bar{\nu}_e$)-pairs increases. The higher the temperature, the more energetic the pairs are. Most (μ, τ)-neutrino pairs are produced at

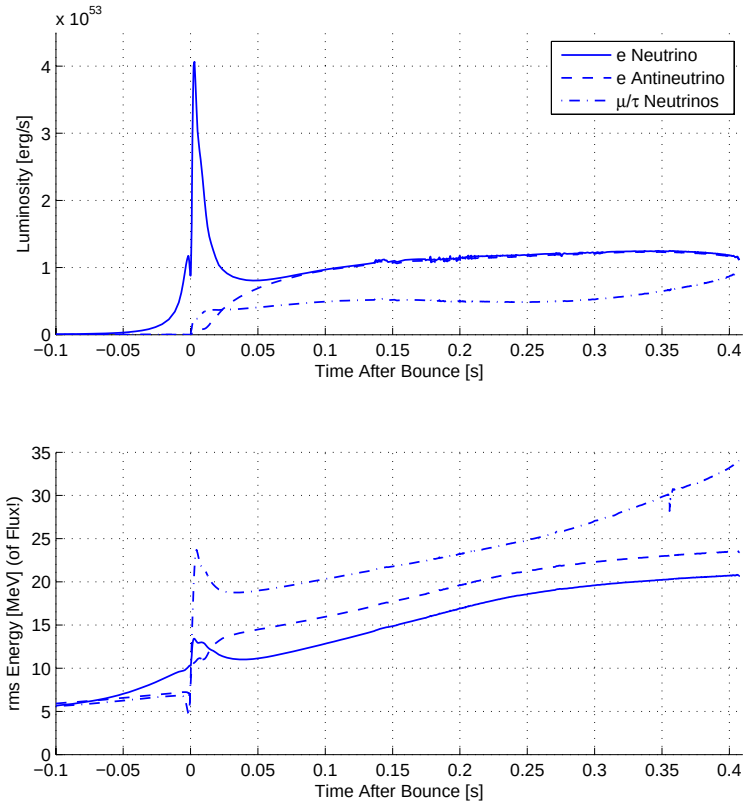

Figure 4.
The graphs illustrate the neutrino luminosities (all flavors) during a core collapse simulation of a $40\,M_{\odot}$ progenitor from Woosley et al. (2002) at $300\,km$ distance. (ν_e, $\bar{\nu}_e$) dominate the early accretion phase, while (ν_μ, ν_τ) as well as their anti-neutrinos become more luminous in the late accretion phase.

$\rho \sim 10^{13} g/cm^3$. This contribution remains rather constant, because the temperature, Y_e and optical depth stay rather constant at that density, as can be seen in graphs (c), (e) and (f) of figure 5. However, at $\rho \sim 10^{11} g/cm^3$ we find a drastic temperature and Y_e increase, which produces a significant rise of the (μ, τ)-neutrino luminosity from lower density as can bee seen in graph (d) of figure 5. Moreover, the diffusion time scale of (μ, τ)-neutrinos is reduced by the compactification of the core. The corresponding decreasing optical depths are shown in graph (c) of figure 5. The electron flavor neutrino luminosities do not rise as significantly, because they are produced via electron and positron capture in layers with lower densities. There, namely at or even outside the neutrino sphere, the temperature increase and Y_e increase are rather small during compactification. Additionally, the optical depth remains almost constant at these lower densities. Indeed, between $250\,ms$ and $350\,ms$ post-bounce the temperature increase and Y_e increase at the (μ, τ)-neutrino-spheres exceed those at the electron flavor neutrino spheres by one order of magnitude, which explains the increase of the $(\nu_{(\mu,\tau)},\bar{\nu}_{(\mu,\tau)})$ luminosity after $300\,ms$ post-bounce, while the $(\nu_e,\bar{\nu}_e)$ luminosity remains almost constant. Note, that the electron flavor neutrino pair-production rate in graph (b) of figure 5 is less important, since the $(\nu_e,\bar{\nu}_e)$-production rate is dominated by charged current reactions shown in graph (a).

However, since (μ, τ)-neutrinos do not interact via charged current reactions, their influence to revive the shock is rather limited. On the other hand, neutrino scattering reactions contribute to the heating as well. Therefore, neutrino-electron and neutrino-positron scattering become more

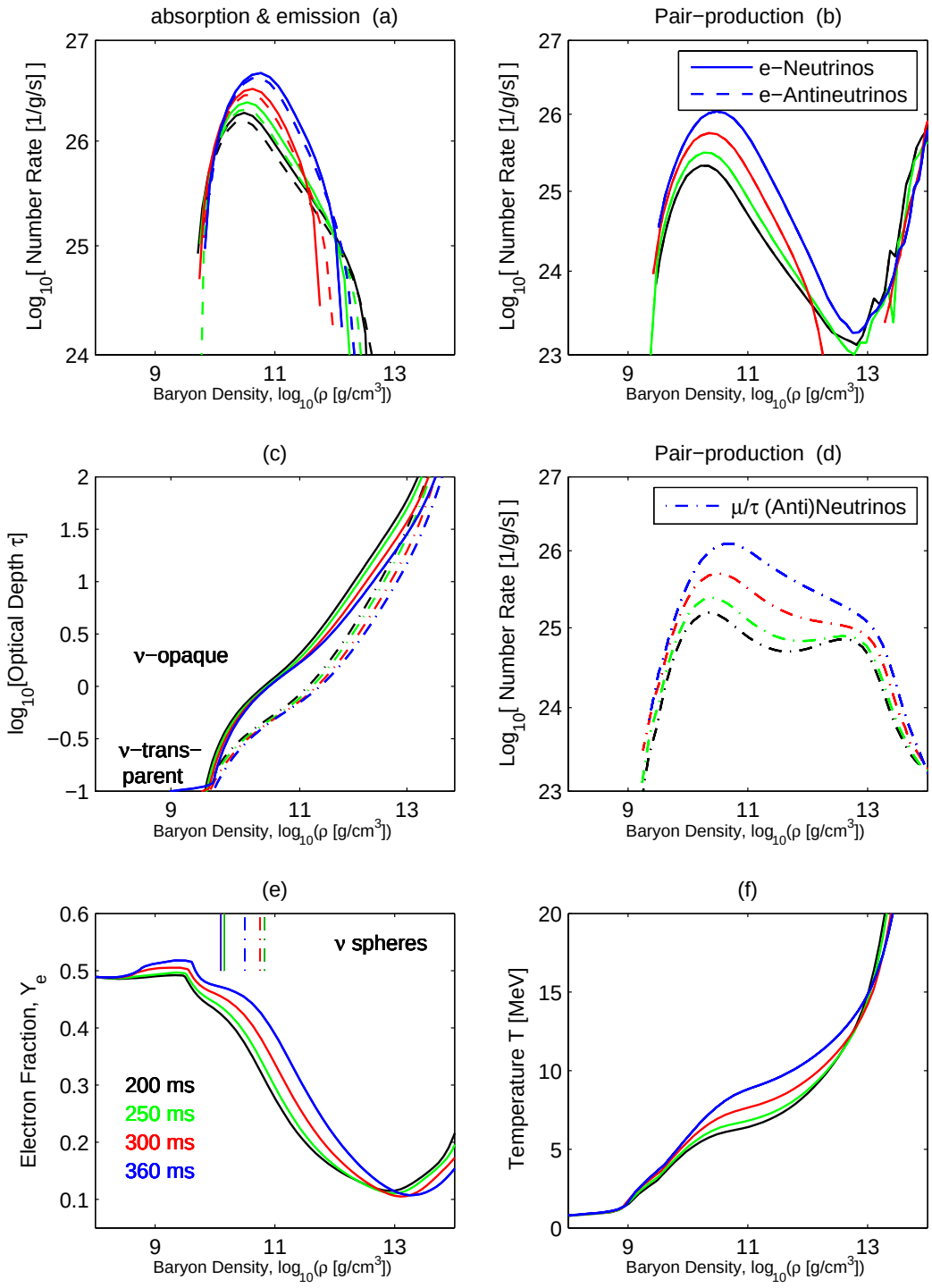

Figure 5.

The graphs show the number fluxes for (ν_e,$\bar{\nu}_e$) emission and absorption as well as pair-production incl. nucleon-nucleon bremsstrahlung for (ν_e,$\bar{\nu}_e$) and ($\nu_{(\mu,\tau)}$,$\bar{\nu}_{(\mu,\tau)}$). In addition, the optical depths are plotted for the mean neutrino energies at about 300 km distance, illustrating the decrease of the distance neutrinos have to diffuse during compactification. The electron fraction and temperature increases most at densities between $10^{10} - 10^{12} g/cm^3$ during compactification which matches the increased production rates in this range.

important in the late accretion phase, with respect to (μ, τ)-neutrino and their anti-neutrino heating between the neutrino spheres and the receding shock. Since the temperature exceeds $150\,MeV$, the continued increase of the energies and luminosities of (μ, τ)-neutrinos as well as their anti-neutrinos in the final accretion phase before PNS collapse might have a positive feedback to revive the shock. In addition, the knowledge of the neutrino signal is of great interest for detecting supernovae via neutrino reactions, learning about the matter conditions involved, being able to decide which type of supernova has been observed and which type of astrophysical object remains.

5. Summary and outlook

We followed the core collapse of a $40\,M_\odot$ progenitor during pre-bounce, bounce, shock formation and post-bounce/accretion phase until the central object, a stable PNS with an initial radius of $50\,km$, was compactified via continued accretion of matter due to a failed explosion, such that it eventually collapses to a black hole. While we used the EoS from Lattimer and Swesty (1991), Sumiyoshi et al. (2006) found interesting differences in the black hole formation timescale, comparing different EoSs. But not only different EoS result in different timescales for black hole formation, also different accretion rates due to initially different progenitor masses cause such an effect. However, the PNS collapse to a black hole itself happens along very similar lines for initially different progenitors. The hydrostatic structure as well as the critical mass of the PNS are mainly determined by the EoS, while the evolution is determined by the progenitor dependent accretion rate. Hence, similar conditions are assumed at different times in comparison of a $40\,M_\odot$ and a $15\,M_\odot$ collapse model. Differences appear mainly with respect to time scales.

Special attention was devoted to the late accretion phase and the formation of the black hole itself. The PNS starts to collapse about $407\,ms$ after bounce and the event horizon is formed at about $409\,ms$ after bounce, stating the very short timescale for black hole formation via PNS collapse. The physical state during PNS collapse is quite unique, highest infall velocities ($\sim c$), temperatures ($190\,MeV$) and densities ($5 \times 10^{15} g/cm^3$) were found.

In addition, the neutrino-signal of all flavors was discussed. During the compactification of the central layers of the stellar core, the $(\nu_e, \bar{\nu}_e)$-signal was found to be almost constant and decreasing at black hole formation, while the $(\nu_{(\mu,\tau)}, \bar{\nu}_{(\mu,\tau)})$-signal increases strongly, starting about $250\,ms$ after bounce and extending to black hole formation. Further improvements are necessary to investigate the neutrino signal of the accreting matter after black hole formation.

Magnetic fields and rotation could affect the PNS collapse and it could be interesting to explore the influence of electromagnetic phenomena and gravitational wave emission at black hole formation. More fundamentally, improvements of the input physics for PNSs at conditions during black hole formation are necessary, to specify more accurately the fate of PNSs that result as central accreting objects in core collapse models without explosions.

References

Akiyama S, Wheeler J C, Meier D L and Lichtenstadt I 2003 *Astrophys. J.* **584** 954-970
Beacom J F, Boyd R N and Mezzacappa A 2001 *Phys. Rev.* D **63** 073011
Bethe H A and Wilson J R 1985 *Astrophys. J.* **295** 14-23
Bruenn S W and Haxton W C 1991 *Astrophys. J.* **376** 678-700
Bruenn S W, Dirk J C, Mezzacappa A, Hayes J C, Blondin J M, Hix W R and Messer O E B 2006 *Journal of Physics: Conference Series* **46** 393-402
Buras R, Janka H-TH, Keil M Th, Raffelt G G and Rampp M 2003 *Astrophys. J.* **587** 320-326
Buras R, Rampp M, Janka H-Th and Kifondis K 2006 *Astronomy and Astrophysics* **447** 1049-1092
Burrows A 1988 *Astrophys. J.* **334** 891
Burrows A, Hayes J and Fryxell B A 1995 *Astrophys. J.* **450** 830-850
Burrows A, Reddy S and Thompson T A 2006 *Nucl. Phys.* **A 777** 356-394
Burrows A, Livne E, Dessart L, Ott C D and Murphy J 2006 *New Astronomy Reviews* **50** 487-491
Cardall C Y and Mezzacappa A 2003 *Phys. Rev.* D **68** 023006

Herant M, Benz W, Hix W R, Fryer C L and Colgate S A 1994 *Astrophys. J.* **435** 339-361
Janka H-Th, Buras R, Kitaura Joyanes J F, Marek A, Rampp M and Scheck L 2005 *Nucl. Phys.* A **758** 19c-26c
Lattimer J M and Swesty F D 1991 *Nucl. Phys.* A **535** 331-376
Liebendörfer M, Mezzacappa A and Thielemann K F 2001a *Phys. Rev.* D **63** 104003
Liebendörfer M, Mezzacappa A, Thielemann K F, Messer O E B, Hix R W and Bruenn S W 2001b *Phys. Rev.* D **63** 103004
Liebendörfer M, Messer O E B, Mezzacappa A, Bruenn S W, Cardall Y C and Thielemann K F 2004 *Astrophys. J. Suppl.* **150** 263-316
Lindquist R W 1966 *Annals of Physics* **37** 487-518
May M M and White E H 1967 *J. Comput. Phys.* **7** 219
Messer O E B and Bruenn S W 2003 private communications
Mezzacappa A and Bruenn S W 1993a *Astrophys. J.* **405** 637-668
Mezzacappa A and Bruenn S W 1993b *Astrophys. J.* **405** 669-684
Mezzacappa A and Bruenn S W 1993c *Astrophys. J.* **410** 710-760
Mezzacappa A and Messer O E B 1999 *Journal of Computational and Applied Mathematics* **109** 281-319
Misner C M and Sharp D H 1964 *Phys. Rev.* **136** B571
Schinder P J and Shapiro S L 1982 *Astrophys. J.* **259** 311-329
Schinder P J and Shapiro S L 1982 *Astrophys. J. Suppl.* **50** 23-38
Schinder P J and Shapiro S L 1986 *Lecture Notes in Physics* **255** 121, Proceedings of IAU Colloq. **89**
Sumiyoshi A, Yamada S, Suzuki H and Chiba S 2006 *Phys. Rev. Lett.* **97** 091101
Wilson J R 1971 *Astrophys. J.* **163** 209
Woosley S, Heger A and Weaver T A 2002 *Reviews of Modern Physics* **74** 1015
Yueh W R and Buchler J R 1975 *Astrophys. J. Suppl.* **39** 429
Yueh W R and Buchler J R 1977 *Astrophys. J.* **217** 565-577